ACS Photonics

Letter

Cite This: ACS Photonics 2019, 6, 838–843

pubs.acs.org/journal/apchd5

Real-Time Tunable Strong Coupling: From Individual Nanocavities to Metasurfaces

Jiani Huang,[†,‡] Andrew J. Traverso,[†,‡] Guoce Yang,[§] and Maiken H. Mikkelsen*[,†,§]

[†]Department of Physics and [§]Department of Electrical and Computer Engineering, Duke University, Durham, North Carolina 27708, United States

Supporting Information

ABSTRACT: Strong light−matter coupling, characterized by a coherent exchange of energy between an emitter and cavity, plays an important role in, for example, quantum information science and thresholdless lasing. To achieve strong coupling, precise spatial and spectral overlap between the emitter and cavity is required, presenting a significant challenge to move from individually strongly coupled cavities to a large number of cavity-coupled systems, as required for future practical applications. Here we demonstrate a versatile platform for realizing strong coupling that scales uniformly from individual nanocavities up to millimeter-scale metasurfaces, while the coupling strength can be tuned dynamically. Fluorescent dye molecules are sandwiched between silver nanocubes and a metallic film creating a plasmonic cavity with a mode volume of only ~0.002 $(\lambda/n)^3$. A prominent anticrossing behavior is observed which corresponds to a large Rabi splitting energy of 152 meV. The plasmon resonance can be tuned up to 45 nm (~210 meV) enabling real-time control of the Rabi splitting as well as tuning from the weak to the strong coupling regime. This scalable, easily fabricated structure opens the door for use in integrated on-chip nanophotonic devices.

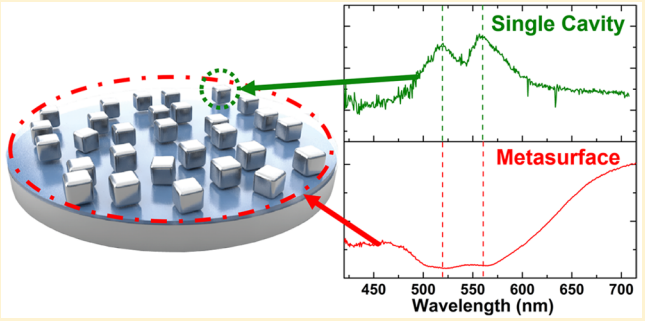

KEYWORDS: *strong coupling, plasmonics, nanocube, active control, metasurfaces*

Probing the interaction between quantum emitters and an optical cavity is crucial to both fundamental studies in cavity-quantum electrodynamics,[1] as well as for potential applications such as thresholdless polariton lasing,[2,3] quantum information storage,[4−6] and ultrafast single-photon switches.[7,8] Strong coupling occurs when a quantum emitter and an optical cavity exchange energy much faster than other competing dissipation rates in the system, enabling coherent and reversible energy transfer between the emitter and the cavity.[9−11] Consequently, this light−matter strong coupling leads to the generation of two new hybrid eigenstates separated by the so-called Rabi splitting, which can be observed in the optical spectra of the hybrid structure (Figure 1a). While the square root of the ratio of the quality factor, Q, and the mode volume, V, is proportional to the coupling strength of the cavity, $\sqrt{Q/V}$,[11−13] the dimensions of conventional optical cavities[9,14] are restricted by the diffraction limit to around half the wavelength of the interacting photons. Thus, for conventional cavities with a modest mode volume, a large quality factor is required to attain strong coupling corresponding to narrow cavity line widths. This makes it challenging to overlap the dipole transition with a particular cavity resonance and often requires extreme experimental conditions such as cryogenics and ultranarrow frequency light sources,[12] which proves even more challenging for a large number of cavity-coupled systems. Alternatively, plasmonic nanocavities enable tiny mode volumes by concentrating electromagnetic fields to deep subwavelength regions by the excitation of surface plasmons.[15−18] While these cavities are intrinsically lossy, the mode volumes can be orders of magnitude smaller than for conventional dielectric cavities, making them intriguing systems for strong coupling. To date, strong coupling has been demonstrated in a number of different plasmonic nanocavities coupled to fluorescent molecules,[13,19−23] quantum dots,[12] two-dimensional materials,[11,24−28] and other nanostructures.[29] Active control of the coupling strength has been demonstrated with photoswitchable molecules,[30−33] polarization-dependent coupling between J-aggregates and gold dimers,[19,34] as well as electrostatic gating and thermal tuning of monolayer transition metal dichalcogenides.[11,35−38] However, extensive nanofabrication was required for precise alignment of the emitters with the cavity, limiting the demonstrations to either single or few cavities.[39]

Here, we demonstrate a straightforward, easily fabricated design that can be tailored to achieve any desired coupling strength up to 152 meV. Furthermore, active thermal tuning is also demonstrated of the cavity-dipole coupling by modification of the plasmon resonance of up to 210 meV. The plasmonic structure used here enables a mode volume of only ~0.002 $(\lambda/n)^3$ by sandwiching an anionic fluorescent dye (Atto 532)

Received: December 18, 2018
Published: March 15, 2019

DOI: 10.1021/acsphotonics.8b01743
ACS Photonics 2019, 6, 838−843

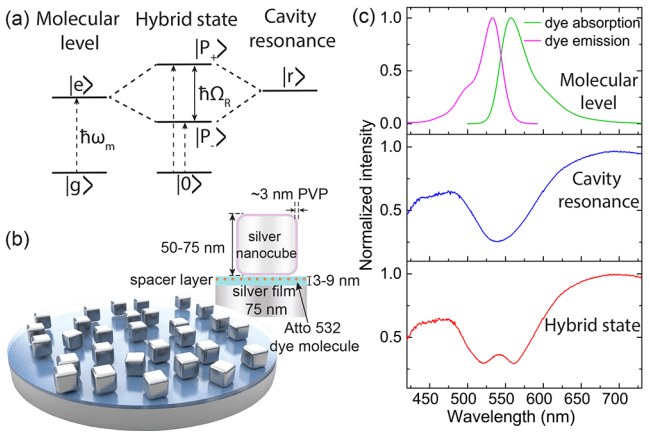

Figure 1. Sample schematic and characterization. (a) Schematic energy diagram of strong coupling between an emitter and an optical cavity, leading to the formation of two new hybrid states separated by the Rabi splitting, $\hbar\Omega_R$. (b) Schematics of the plasmonic structure, which consists of silver nanocubes placed over a silver film and separated by a nanoscale spacer layer consisting of dye molecules and polymer. (c) Top: absorption and emission spectra of the dye molecule Atto 532; middle: reflectance spectrum showing the fundamental resonance of the cavity when the dye molecules are uncoupled; bottom: a clear mode splitting can be seen in the reflectance spectrum when the dye molecules are coupled to the plasmonic cavity.

embedded in alternately charged polyelectrolyte (PE) layers between colloidally synthesized silver nanocubes and a template-stripped silver film (Figure 1b). Given the charged nature of the PE layers and dye, the dipole orientation of the dye is likely close to normal to the surface.[40,41] The absorption of the fluorescent dye at 532 nm and emission at 560 nm are spectrally close (top panel, Figure 1c), enabling a single mode of the plasmonic cavity to overlap with and enhance both processes. A dense metasurface of these gap-plasmon resonators[42] was fabricated over a 12 mm diameter area with an average spacing of 194 nm between nanocubes. For a 7 nm PE spacer layer and 60 nm cubes, the plasmonic cavity shows a fundamental resonance at 550 nm, overlapping with both the absorption and emission of the dye (middle panel, Figure 1c). When the dye molecules are coupled to the cavity, a mode splitting is observed in the spectra as seen in the bottom panel of Figure 1c.

To verify that the observed mode splitting indeed arises from strong coupling between the dye molecules and the cavity, reflectance spectra were measured from ten metasurfaces with different resonances. By varying the nanocube size and the gap thickness, the plasmon resonance was tuned across the transition energy of the dye molecule while the dye concentration (5 mM) was unchanged (Figure 2a). For dye-coupled cavities, two prominent hybrid modes were observed in all reflectance spectra; however, the strength of each mode was highly dependent on the detuning between the cavity resonance and the dye absorption. When the plasmonic cavity was blue-detuned from the dye transition energy, the higher energy mode (blue) dominated, whereas when the cavity resonance was red-detuned from the dye transition energy, the lower energy mode (red) was more prominent. At zero-detuning, the intensities of the two hybrid modes are comparable. The fundamental plasmon resonance of the metasurfaces was verified by photobleaching the dye molecules in each sample using a high-power laser (~1 kW/cm^2, 532 nm), as shown in Figure 2a. Furthermore, as depicted more clearly in Figure 2b, the cavity detuning also modifies the spectral positions of the hybrid modes. As the plasmon resonance is varied across the dye absorption transition energy, the strongly coupled system exhibits a distinct avoided crossing at zero-detuning. This anticrossing behavior, a hallmark of strong coupling, can be fitted using a coupled harmonic oscillator model, whose energy eigenmodes are defined by[17,26,43]

$$E = \frac{\hbar\omega_{cav} + \hbar\omega_{abs}}{2} + \frac{i\hbar(\gamma_{cav} + \gamma_{abs})}{2} \pm \sqrt{G^2 + \frac{1}{4}(\hbar\omega_{cav} - \hbar\omega_{abs} + i\hbar\gamma_{cav} - i\hbar\gamma_{abs})^2} \quad (1)$$

where $\hbar\omega_{abs}$ and $\hbar\omega_{cav}$ are the energies for the dye absorption and the cavity resonance, respectively, while γ_{abs} and γ_{cav} are the half-width at half-maximum (HWHM) line widths of these resonances, and G is the coupling strength between the dye absorption and the plasmonic cavity. When $\omega_{abs} = \omega_{cav}$, the Rabi splitting is given by

$$\hbar\Omega_R = 2\sqrt{G^2 - (\hbar^2/4)(\gamma_{cav} - \gamma_{abs})^2}$$

As depicted in the solid lines in Figure 2b, the model shows good agreement with the experimental data, providing a fitted coupling strength, G, of approximately 107 meV and a Rabi splitting energy of 152 meV. Given the HWHM line widths of the dye absorption and plasmonic cavity resonances of 65 and 215 meV, respectively, this satisfies the condition of $2G > \hbar|\gamma_{cav} - \gamma_{abs}|$ for strong coupling.[43] Although this is the standard criterion for strong coupling, it is not the only benchmark. An

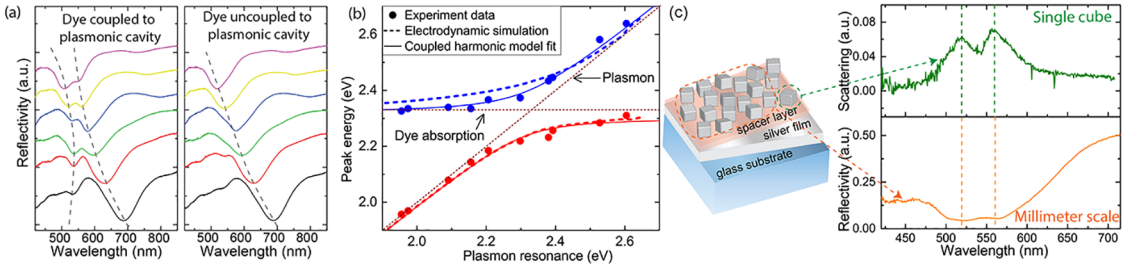

Figure 2. Strong coupling and anticrossing behavior. (a) Reflectance spectra for dye coupled and uncoupled to the plasmonic cavity at varying plasmon resonances. The resonance is tuned by either varying the nanocube size or the gap thickness. The dye was uncoupled from the cavity by photobleaching it via a 1 min exposure with a focused 532 nm laser. (b) A clear anticrossing behavior is observed, which agrees well with both full-wave electrodynamic simulations performed by COMSOL Multiphysics (dashed) and coupled harmonic oscillator model fits (solid), as defined in eq 1. The horizontal dashed line represents the absorption energy of the dye. The tilted dashed line represents the plasmon resonance (c) Scattering from an individual plasmonic cavity and reflectance from a millimeter-scale area of the metasurface, both showing strong coupling mode splitting.

DOI: 10.1021/acsphotonics.8b01743
ACS Photonics 2019, 6, 838−843

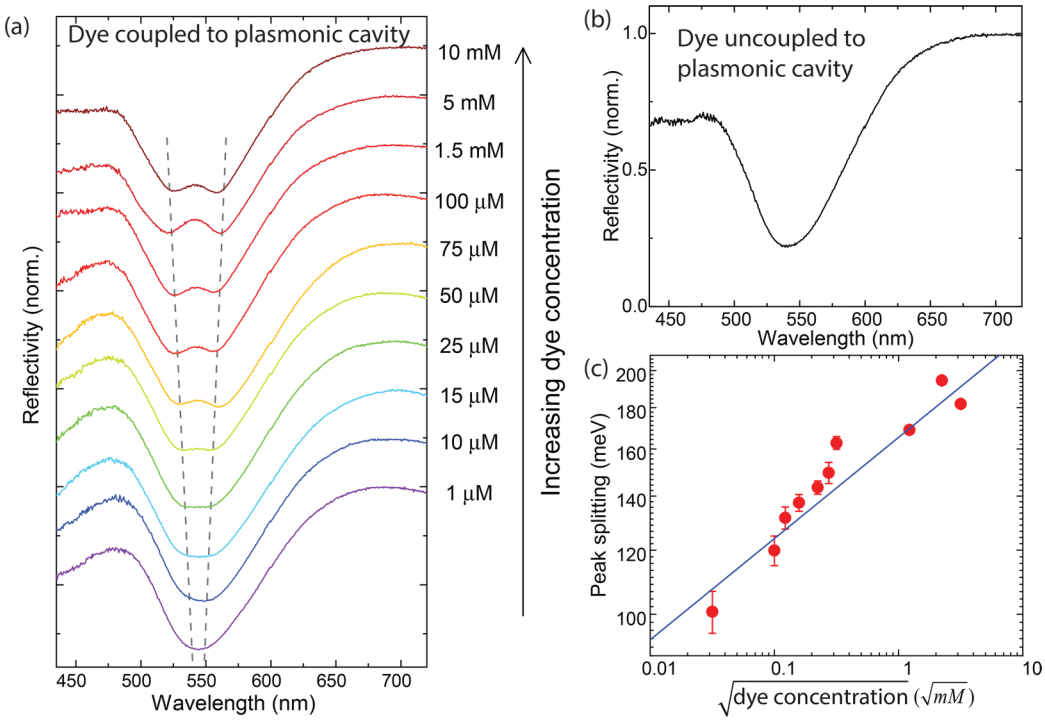

Figure 3. Tuning of dye concentration. (a) Reflectance spectra of dye coupled to the plasmonic cavity for varying dye concentrations. The splitting becomes larger as the dye concentration increases. (b) Reflectance spectra of dye uncoupled to the plasmonic cavity, showing a fundamental resonance at 541 nm. (c) The extracted peak splitting energy as a function of the square root of the dye concentration. The solid line is a fit to eq 2.

alternative approach compares the Rabi splitting energy with the average full-width at half-maximum (fwhm) of the modes, which for this system are 152 and 280 meV, respectively. While typically the Rabi splitting should be greater than the average fwhm of the line widths, given that the parameters are on the same order of magnitude, this is still within the strong coupling regime. For this instead to be a Fano-resonance, there would need to be a greater mismatch by at least an order of magnitude between the dye and the cavity line widths. These aspects in conjunction with the large coupling strength of 107 meV and satisfying the standard definition confirms that the splitting observed in our experiment is due to strong coupling between the dye molecules and the plasmonic cavity mode.

Additionally, full-wave simulations of the electrodynamics were performed using a finite-element method (COMSOL Multiphysics) and are shown in the dashed curves in Figure 2b. For these simulations, the effective oscillator strength was tuned to achieve good agreement with experiment, whereas other parameters such as the geometry of the structure and optical properties of the constituent materials utilized measured or known values. These results, when fitted with the coupled oscillator model, reveal a coupling strength, G, and a Rabi splitting of 94 and 162 meV, respectively, in good agreement to the experimental fittings. Overall, there is good agreement between the coupled-oscillator model, the full-wave simulations performed by COMSOL Multiphysics, and the experimental data confirming the presence of strong coupling. It should be noted that the line widths of the two hybrid modes are broader when measured from a metasurface versus from an individual nanocavity, as depicted in Figure 2c. This is likely due to slight variations in the thickness of the gap and nanocube size, both of which modify the plasmon resonance measured from a metasurface. Further details on the simulations can be found in the Supporting Information.

To confirm if the strong coupling observed for metasurfaces scales down to single nanoscale plasmonic cavities, dark-field scattering measurements were performed. A representative measurement shown in Figure 2c demonstrates that strong coupling can indeed be measured from single nanocavities and occurs at approximately the same Rabi splitting energy as seen for the large-area metasurface. Thus, this system exhibits a uniform coupling strength that scales from the individual nanometer-scale cavity up to a region of several millimeters.

In addition to the dimensions of the nanocavity and detuning of the plasmon resonance, the coupling strength also depends on the number of coupled molecules, N, as follows:[11,13]

$$G = \mu_{\mathrm{m}}\sqrt{\frac{4\pi\hbar Nc}{\lambda\varepsilon\varepsilon_0 V}} \tag{2}$$

where μ_{m} is the transition dipole moment of the molecules, V is the mode volume of the cavity, ε is the dielectric function, and λ is the wavelength. Thus, for a plasmonic cavity with fixed dimensions and type of emitters, the coupling strength, G, should be linearly dependent on $\sqrt{N}$. To gain more insight into the relationship between the coupling strength and the number of molecules, we investigate the reflectance spectra of the coupled system as a function of dye concentration while maintaining the same plasmon resonance and nanocavity dimensions. The results depicted in Figure 3a demonstrate that as the dye concentration increases, the Rabi energy splitting also increases where the high- and low-energy modes blue- and red-shift, respectively. The symmetrical shifting of both modes is largely due to the zero detuning of the cavity resonance at 550 nm with the dye absorption (Figure 3b). For a more quantitative understanding of the coupling strength, we extract the energy splitting between the hybrid modes in each spectrum and fit them as a function of the square root of the dye concentration

DOI: 10.1021/acsphotonics.8b01743
ACS Photonics 2019, 6, 838−843

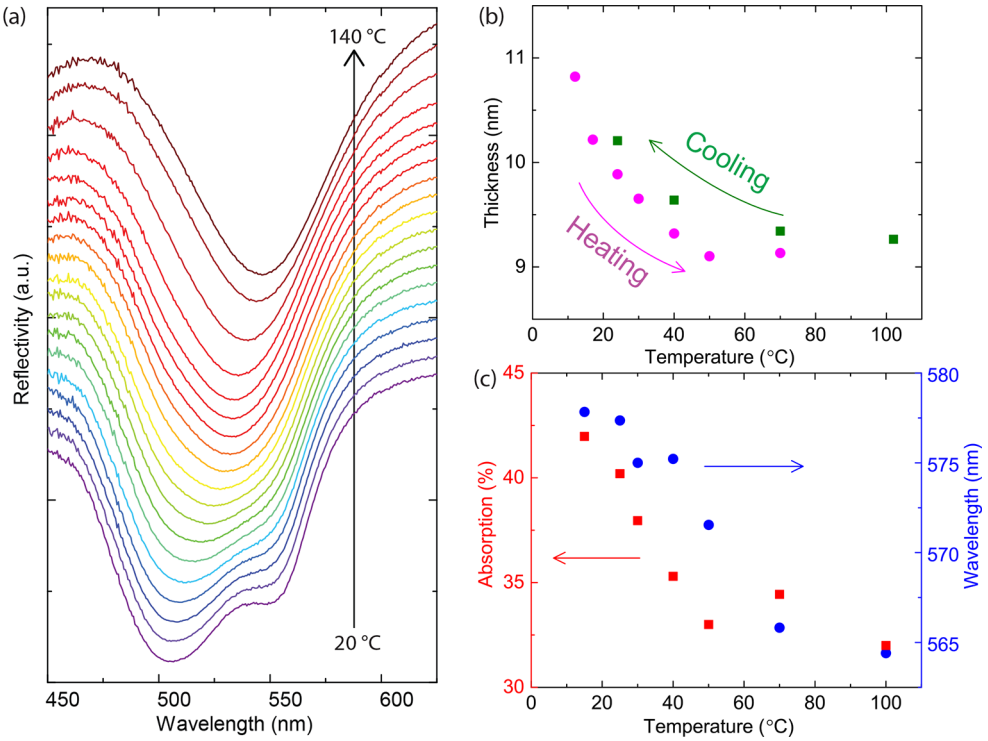

Figure 4. Temperature tuning of strong coupling. (a) Reflectance spectra when the temperature is tuned from 20 to 140 °C for a dye concentration of 5 mM. The resonance is red-shifted as the temperature increases. The resonance is tuned up to 45 nm (210 meV), though the coupling strength decreases. (b) Temperature dependence of the thickness of the polymer spacer layer (9 PAH and PSS layers) measured by ellipsometer for both heating (purple circles) and cooling (green squares). As the temperature increases, the thickness decreases due to water removal and reentry during heating and cooling, respectively. (c) Temperature dependence of the dye absorption. As the temperature increases, the dye absorption intensity decreases, while the absorption blue-shifts.

using eq 2. As seen in Figure 3c, a linear relationship is obtained, which is consistent with the theory showing $G \propto \sqrt{N}$. Based on prior studies,[44] we estimate that less than 5% of the dye is adsorbed on the surface, which for a concentration of 75 μM, corresponds to less than 500 dye molecules underneath each cube at an average spacing of approximately 5 nm. Using eq 2 in conjunction with the fitted coupling strength of G = 107 meV, the calculated dipole moment μ_m,[45] an estimate of the cavity mode volume $V \sim 0.002\ (\lambda/n)^3$ based on the dimensions of the gap volume, and the index of refraction of PAH/PSS (~1.48),[46] the estimated number of dipoles, N, is approximately 450. This is in close agreement with the estimate based on dye adsorption. Furthermore, returning to the fitted coupling strength from the full-wave simulations performed by COMSOL Multiphysics, G = 93 meV, we can use the approximate value for N to estimate the dipole moment, μ_m, to be 7.2 D. This estimate is in good qualitative agreement with the theoretical 8.2 D value derived from manufacturer-provided emission lifetime in solution.[45] It should be noted that eq 2 does not account for the spatial variation of the electric field enhancement. While this would alter the estimated number of emitters, N, it would also alter the estimated mode volume, V, because the few emitters which strongly contribute to the Rabi splitting in the highest field enhancement only occupy a subsection of the volume in the gap. Given that the dye distribution, (N/V), is likely fairly uniform, we expect that our use of a uniform field enhancement and the total gap volume as V, provides a close estimate that shows good qualitative agreement with known parameters. Furthermore, it is assumed that the dipole orientation of the anionic dye is oriented normal to the surface,[40,41] any angular deviation will change the estimated N. While accounting for these aspects could potentially improve the accuracy of the estimates, eq 2 provides an intuitive, general understanding of the coupling strength in the plasmonic cavity.

Next, we demonstrate active tuning of the plasmon resonance of the metasurface and, in turn, the coupling strength. In particular, we designed the metasurface with a 9 nm gap thickness and a nanocube size of 55 nm such that the plasmon resonance at 510 nm is blue-detuned from the dye absorption. The metasurface was actively heated/cooled over a 120 °C range to achieve dynamic control of the coupling strength by spectral detuning of the plasmon resonance over 45 nm (~210 meV), as seen in Figure 4a. In this system, the detuning changes due to the temperature sensitivity of the PE polymer spacer layers, leading to the shift in the plasmon resonances. Furthermore, the light–matter coupling also changes arising from the temperature tuning of the absorption properties of the dye molecules. As determined by ellipsometry measurements shown in Figure 4b, the thickness of the PE spacer layer, that is, PAH and PSS polymers, is highly dependent on the temperature, which in turn modifies the nanocavity resonance.[47] Specifically, an increase in the temperature decreases the relative humidity, which results in a thinning of the spacer layers and an increase in the index of refraction,[46] which subsequently causes the plasmon resonance to red-shift; similarly, a decrease in the temperature leads to a blue-shifted cavity resonance. This change in film thickness is likely due to the removal of water from the film and subsequent reentry during heating and cooling, respectively.[48] In contrast to the plasmon resonance, the spectral absorption of the dye molecule blue-shifts and weakens with increasing temperature,

DOI: 10.1021/acsphotonics.8b01743
ACS Photonics 2019, 6, 838–843

as seen in Figure 4c. Given the opposite temperature responses and weakening absorption with increasing temperature, it is possible to tune the coupled system out of the strong coupling regime and revert to simply a single mode defined by the fundamental plasmon resonance. This is depicted clearly in Figure 4a, where the low-energy hybrid mode becomes less prominent as the temperature increases. We should also note that there is some hysteresis for the dynamic thermal tuning such that if the metasurface has been heated or cooled and then allowed to revert to its original temperature, the resulting reflectance spectrum is spectrally shifted by a few nanometers from the original spectrum. This hysteresis disappears if the sample is allowed to sit for a few hours resulting in full reversal back to the originally observed reflectance spectrum. This dynamic tuning approach is in contrast to other demonstrations in that the tuning is mainly the result of shifting the plasmon resonance instead of the coupled dipole,[30] with only a slight temperature variation in the dipole absorption.

In summary, we have demonstrated real-time tunable Rabi splittings up to 152 meV between fluorescent dye molecules and nanogap plasmonic cavities. This strong coupling scales uniformly from the nanoscale with individual deep subwavelength cavities up to macroscopic areas using self-assembled metasurfaces. The plasmon resonance was dynamically tuned over a 45 nm range (~210 meV) enabling the coupling strength between the nanocavities and dye molecules to be tuned from the strong to the weak coupling regime. This points toward future applications of strongly coupled systems with tailored optical properties, including controlled light absorption, scattering or emission. Given the active tuning, ease and simplicity of fabrication, and scalability of the metasurface, these results could lead to novel nanophotonic devices, including modulators, switches, and sensors.

■ ASSOCIATED CONTENT

Supporting Information

The Supporting Information is available free of charge on the ACS Publications website at DOI: 10.1021/acsphotonics.8b01743.

Detailed description of the sample fabrication, optical measurements, and simulations (PDF)

■ AUTHOR INFORMATION

Corresponding Author

*E-mail: m.mikkelsen@duke.edu.

ORCID

Maiken H. Mikkelsen: 0000-0002-0487-7585

Author Contributions

‡These authors contributed equally to this work.

Author Contributions

M.H.M. proposed and designed the experiment and supervised the project. J.H. and A.J.T. fabricated the samples, performed the experiments, and analyzed the data. G.Y. performed the simulations. All authors contributed to the writing of the manuscript.

Notes

The authors declare no competing financial interest.

■ ACKNOWLEDGMENTS

This work was supported by a Cottrell Scholar award from the Research Corporation for Science Advancement and a Faculty Early Career Development Program (CAREER) award from the National Science Foundation (DMR-1454523). G.Y. acknowledges support from the China Scholarship Council (CSC, No. 201606210320).

■ REFERENCES

(1) Mabuchi, H.; Doherty, A. C. Cavity Quantum Electrodynamics: Coherence in Context. *Science* **2002**, *298*, 1372−1377.

(2) Christopoulos, S.; Von Högersthal, G. B. H.; Grundy, A. J. D.; Lagoudakis, P. G.; Kavokin, A. V.; Baumberg, J. J.; Christmann, G.; Butté, R.; Feltin, E.; Carlin, J. F.; et al. Room-Temperature Polariton Lasing in Semiconductor Microcavities. *Phys. Rev. Lett.* **2007**, *98*, 126405.

(3) Kéna-Cohen, S.; Forrest, S. R. Room-Temperature Polariton Lasing in an Organic Single-Crystal Microcavity. *Nat. Photonics* **2010**, *4*, 371−375.

(4) Sillanpää, M. A.; Park, J. I.; Simmonds, R. W. Coherent Quantum State Storage and Transfer between Two Phase Qubits via a Resonant Cavity. *Nature* **2007**, *449*, 438−442.

(5) Hennessy, K.; Badolato, A.; Winger, M.; Gerace, D.; Atatüre, M.; Gulde, S.; Fält, S.; Hu, E. L.; Imamoğlu, A. Quantum Nature of a Strongly Coupled Single Quantum Dot−cavity System. *Nature* **2007**, *445*, 896−899.

(6) Monroe, C. Quantum Information Processing with Atoms and Photons. *Nature* **2002**, *416*, 238−246.

(7) Volz, T.; Reinhard, A.; Winger, M.; Badolato, A.; Hennessy, K. J.; Hu, E. L.; Imamoğlu, A. Ultrafast All-Optical Switching by Single Photons. *Nat. Photonics* **2012**, *6*, 605−609.

(8) Chen, W.; Beck, K. M.; Bücker, R.; Gullans, M.; Lukin, M. D.; Tanji-Suzuki, H.; Vuletić, V. All-Optical Switch and Transistor Gated by One Stored Photon. *Science* **2013**, *341*, 768−770.

(9) Yoshie, T.; Scherer, A.; Hendrickson, J.; Khitrova, G.; Gibbs, H. M.; Rupper, G.; Ell, C.; Shchekin, O. B.; Deppe, D. G. Vacuum Rabi Splitting with a Single Quantum Dot in a Photonic Crystal Nanocavity. *Nature* **2004**, *432*, 9−12.

(10) Koenderink, A. F.; Alù, A.; Polman, A. Nanophotonics: Shrinking Light-Based Technology. *Science* **2015**, *348*, 516−521.

(11) Wen, J.; Wang, H.; Wang, W.; Deng, Z.; Zhuang, C.; Zhang, Y.; Liu, F.; She, J.; Chen, J.; Chen, H.; et al. Room-Temperature Strong Light-Matter Interaction with Active Control in Single Plasmonic Nanorod Coupled with Two-Dimensional Atomic Crystals. *Nano Lett.* **2017**, *17*, 4689−4697.

(12) Santhosh, K.; Bitton, O.; Chuntonov, L.; Haran, G. Vacuum Rabi Splitting in a Plasmonic Cavity at the Single Quantum Emitter Limit. *Nat. Commun.* **2016**, *7*, 11823.

(13) Chikkaraddy, R.; Nijs, B. De; Benz, F.; Barrow, S. J.; Scherman, O. A.; Fox, P. Single-Molecule Strong Coupling at Room Temperature in Plasmonic Nanocavities. *Nature* **2016**, *535*, 127−130.

(14) Reithmaier, J. P.; Sek, G.; Löffler, A.; Hofmann, C.; Kuhn, S.; Reitzenstein, S.; Keldysh, L. V.; Kulakovskii, V. D.; Reinecke, T. L.; Forchel, A. Strong Coupling in a Single Quantum Dot-Semiconductor Microcavity System. *Nature* **2004**, *432*, 197−200.

(15) Pelton, M.; Aizpurua, J.; Bryant, G. Metal-Nanoparticle Plasmonics. *Laser Photonics Rev.* **2008**, *2*, 136−159.

(16) Schuller, J. A.; Barnard, E. S.; Cai, W.; Jun, Y. C.; White, J. S.; Brongersma, M. L. Plasmonics for Extreme Light Concentration and Manipulation. *Nat. Mater.* **2010**, *9*, 193−204.

(17) Törmö, P.; Barnes, W. L. Strong Coupling between Surface Plasmon Polaritons and Emitters: A Review. *Rep. Prog. Phys.* **2015**, *78*, 013901.

(18) Halas, N. J.; Lal, S.; Chang, W. S.; Link, S.; Nordlander, P. Plasmons in Strongly Coupled Metallic Nanostructures. *Chem. Rev.* **2011**, *111*, 3913−3961.

(19) Schlather, A. E.; Large, N.; Urban, A. S.; Nordlander, P.; Halas, N. J. Near-Field Mediated Plexcitonic Coupling and Giant Rabi Splitting in Individual Metallic Dimers. *Nano Lett.* **2013**, *13*, 3281−3286.

DOI: 10.1021/acsphotonics.8b01743
ACS Photonics 2019, 6, 838−843

(20) Kato, F.; Minamimoto, H.; Nagasawa, F.; Yamamoto, Y. S.; Itoh, T.; Murakoshi, K. Active Tuning of Strong Coupling States between Dye Excitons and Localized Surface Plasmons via Electrochemical Potential Control. *ACS Photonics* **2018**, *5*, 788−796.
(21) Liu, R.; Zhou, Z. K.; Yu, Y. C.; Zhang, T.; Wang, H.; Liu, G.; Wei, Y.; Chen, H.; Wang, X. H. Strong Light-Matter Interactions in Single Open Plasmonic Nanocavities at the Quantum Optics Limit. *Phys. Rev. Lett.* **2017**, *118*, 237401.
(22) Fofang, N. T.; Grady, N. K.; Fan, Z.; Govorov, A. O.; Halas, N. J. Plexciton Dynamics: Exciton-Plasmon Coupling in a J-Aggregate-Au Nanoshell Complex Provides a Mechanism for Nonlinearity. *Nano Lett.* **2011**, *11*, 1556−1560.
(23) Fofang, N. T.; Park, T.; Neumann, O.; Mirin, N. A.; Nordlander, P.; Halas, N. J. Plexcitonic Nanoparticles: Plasmon - Exciton Coupling in Nanoshell - J-Aggregate Complexes. *Nano Lett.* **2008**, *8*, 3481−3487.
(24) Flatten, L. C.; Christodoulou, S.; Patel, R. K.; Buccheri, A.; Coles, D. M.; Reid, B. P. L.; Taylor, R. A.; Moreels, I.; Smith, J. M. Strong Exciton-Photon Coupling with Colloidal Nanoplatelets in an Open Microcavity. *Nano Lett.* **2016**, *16*, 7137−7141.
(25) Liu, X.; Bao, W.; Li, Q.; Ropp, C.; Wang, Y.; Zhang, X. Control of Coherently Coupled Exciton Polaritons in Monolayer Tungsten Disulphide. *Phys. Rev. Lett.* **2017**, *119*, No. 027403.
(26) Liu, X.; Galfsky, T.; Sun, Z.; Xia, F.; Lin, E. C.; Lee, Y. H.; Kéna-Cohen, S.; Menon, V. M. Strong Light-Matter Coupling in Two-Dimensional Atomic Crystals. *Nat. Photonics* **2015**, *9*, 30−34.
(27) Wang, S.; Li, S.; Chervy, T.; Shalabney, A.; Azzini, S. Coherent Coupling of WS_2 Monolayers with Metallic Photonic Nanostructures at Room Temperature. *Nano Lett.* **2016**, *16*, 4368−4374.
(28) Dufferwiel, S.; Schwarz, S.; Withers, F.; Trichet, A. A. P.; Li, F.; Sich, M.; Del Pozo-Zamudio, O.; Clark, C.; Nalitov, A.; Solnyshkov, D. D.; et al. Exciton-Polaritons in van Der Waals Heterostructures Embedded in Tunable Microcavities. *Nat. Commun.* **2015**, *6*, 8579.
(29) Day, J. K.; Large, N.; Nordlander, P.; Halas, N. J. Standing Wave Plasmon Modes Interact in an Antenna-Coupled Nanowire. *Nano Lett.* **2015**, *15*, 1324−1330.
(30) Schwartz, T.; Hutchison, J. A.; Genet, C.; Ebbesen, T. W. Reversible Switching of Ultrastrong Light-Molecule Coupling. *Phys. Rev. Lett.* **2011**, *106*, 196405.
(31) Baudrion, A. L.; Perron, A.; Veltri, A.; Bouhelier, A.; Adam, P. M.; Bachelot, R. Reversible Strong Coupling in Silver Nanoparticle Arrays Using Photochromic Molecules. *Nano Lett.* **2013**, *13*, 282−286.
(32) Lin, L.; Wang, M.; Wei, X.; Peng, X.; Xie, C.; Zheng, Y. Photoswitchable Rabi Splitting in Hybrid Plasmon − Waveguide Modes. *Nano Lett.* **2016**, *16*, 7655−7663.
(33) Berrier, A.; Cools, R.; Arnold, C.; Offermans, P.; Crego-Calama, M.; Brongersma, S. H.; Gómez-Rivas, J. Active Control of the Strong Coupling Regime between Porphyrin Excitons and Surface Plasmon Polaritons. *ACS Nano* **2011**, *5*, 6226−6232.
(34) Zhang, K.; Chen, T.-Y.; Shi, W.-B.; Li, C.-Y.; Fan, R.-H.; Wang, Q.-J.; Peng, R.-W.; Wang, M. Polarization-Dependent Strong Coupling between Surface Plasmon Polaritons and Excitons in an Organic-Dye-Doped Nanostructure. *Opt. Lett.* **2017**, *42*, 2834−2837.
(35) Lee, B.; Liu, W.; Naylor, C. H.; Park, J.; Malek, S. C.; Berger, J. S.; Johnson, A. T. C.; Agarwal, R. Electrical Tuning of Exciton-Plasmon Polariton Coupling in Monolayer MoS_2 Integrated with Plasmonic Nanoantenna Lattice. *Nano Lett.* **2017**, *17*, 4541−4547.
(36) Li, B.; Zu, S.; Zhou, J.; Jiang, Q.; Du, B.; Shan, H.; Luo, Y.; Liu, Z.; Zhu, X.; Fang, Z. Single-Nanoparticle Plasmonic Electro-Optic Modulator Based on MoS_2 Monolayers. *ACS Nano* **2017**, *11*, 9720−9727.
(37) Cuadra, J.; Baranov, D. G.; Wersäll, M.; Verre, R.; Antosiewicz, T. J.; Shegai, T. Observation of Tunable Charged Exciton Polaritons in Hybrid Monolayer WS_2-Plasmonic Nanoantenna System. *Nano Lett.* **2018**, *18*, 1777−1785.
(38) Kleemann, M. E.; Chikkaraddy, R.; Alexeev, E. M.; Kos, D.; Carnegie, C.; Deacon, W.; De Pury, A. C.; Große, C.; De Nijs, B.; Mertens, J.; et al. Strong-Coupling of WSe2 in Ultra-Compact Plasmonic Nanocavities at Room Temperature. *Nat. Commun.* **2017**, *8*, 1296.
(39) Fernández-Domínguez, A. I.; Bozhevolnyi, S. I.; Mortensen, N. A. Plasmon-Enhanced Generation of Nonclassical Light. *ACS Photonics* **2018**, *5*, 3447−3451.
(40) Chen, S.; Liu, L.; Zhou, J.; Jiang, S. Controlling Antibody Orientation on Charged Self-Assembled Monolayers. *Langmuir* **2003**, *19*, 2859−2864.
(41) Barritault, P.; Gétin, S.; Chaton, P.; Vinet, F.; Fouqué, B. Determination of Surface-Bound-Fluorophore Orientation by Goniometric Fluorescence Polarization: Application to Quantification of DNA-Chip Readouts. *Appl. Opt.* **2002**, *41*, 4732−4738.
(42) Ding, F.; Yang, Y.; Deshpande, R. A.; Bozhevolnyi, S. I. A Review of Gap-Surface Plasmon Metasurfaces: Fundamentals and Applications. *Nanophotonics* **2018**, *7*, 1129−1156.
(43) *Strong Light-Matter Coupling: From Atoms to Solid-State Systems*; Auffeves, A., Gerace, D., Richard, M., Portolan, S., Santos, M. F., Kwek, L. C., Miniatura, C., Eds.; World Scientific: Hackensack, NJ, 2014.
(44) Reineck, P.; Gómez, D.; Ng, S. H.; Karg, M.; Bell, T.; Mulvaney, P.; Bach, U. Distance and Wavelength Dependent Quenching of Molecular Fluorescence by $Au@SiO_2$ Core-Shell Nanoparticles. *ACS Nano* **2013**, *7*, 6636−6648.
(45) Chung, P.-H.; Tregidgo, C.; Suhling, K. Determining a Fluorophore's Transition Dipole Moment from Fluorescence Lifetime Measurements in Solvents of Varying Refractive Index. *Methods Appl. Fluoresc.* **2016**, *4*, No. 045001.
(46) Wong, J. E.; Rehfeldt, F.; Hänni, P.; Tanaka, M.; Klitzing, R. V. Swelling Behavior of Polyelectrolyte Multilayers in Saturated Water Vapor. *Macromolecules* **2004**, *37*, 7285−7289.
(47) Akselrod, G. M.; Huang, J.; Hoang, T. B.; Bowen, P. T.; Su, L.; Smith, D. R.; Mikkelsen, M. H. Large-Area Metasurface Perfect Absorbers from Visible to Near-Infrared. *Adv. Mater.* **2015**, *27*, 8028−8034.
(48) Lvov, Y.; Decher, G.; Mohwald, M. Assembly, Structural Characterization, and Thermal Behavior of Layer-by-Layer Deposited Ultrathin Films of Poly(Vinyl Sulfate) and Poly(Allylamine). *Langmuir* **1993**, *9*, 481−486.

DOI: 10.1021/acsphotonics.8b01743
ACS Photonics 2019, 6, 838−843